DOI: 10.26599/FSHW.2026.9250922

Contents lists available at SciOpen

Food Science and Human Wellness

journal homepage: https://www.sciopen.com/journal/2097-0765

China Food Publishing Co.

Synthesis, stability, and anti-inflammatory activity of selenium nanoparticles stabilized by lotus root polysaccharide

Ying Sun[1, #, *], Weina Yang[1, #], Na Deng [1], Yang Yi[1, *] and Hongxun Wang[2]

[1]*College of Food Science & Engineering, Wuhan Polytechnic University, Wuhan 430023, China*

[2]*College of Life Science and Technology, Wuhan Polytechnic University, Wuhan 430023, China*

ABSTRACT: In this study, selenium nanoparticles (SeNPs) decorated with lotus root polysaccharide (LR) were successfully synthesized, and the formation, particle size, morphology and stabilization of LR/SeNPs1-5 with different Se content were comprehensively characterized. The findings revealed that LR/SeNPs exhibited uniformly spherical nanoparticles with particle size of approximately 100 nm. FT-IR and XPS spectra showed that the stability of LR/SeNPs was attributed to the formation of C-O···Se coordination bonds and hydrogen bond networks between LR and SeNPs. And the environmental stability experiment has proved that LR/SeNPs3 exhibit excellent stability in normal temperature, neutral and low-salt environments, howerer, to maintain long-term stability, it is necessary to avoid from high temperatures, high acidity and high salt environments. Also, the modification of the SeNPs with LR granted the LR/SeNPs excellent anti-inflammatory capability, that decreased the level of NO, IL-1β and TNF-α, and promoted macrophage toward the M2 phenotype polarization, during which LR showed a synergistic effect. These results suggest that LR can not only enhance the stability of SeNPs, but also improve the anti-inflammatory activity of SeNPs, thereby functioning as a promising stabilizing agent for SeNPs.

Keywords: lotus root polysaccharide, SeNPs, stability, anti-inflammatory activity.

1. Introduction

Selenium (Se) is an important trace element for human physiological functions and a natural antioxidant, playing an indispensable role in various biological processes[1, 2]. However, organisms are unable to synthesize Se on their own, and the sole route to obtain Se is through dietary intake[3]. Sodium selenite, methyl selenium, and selenomethionine are among the most commonly used Se sources. However, the extremely narrow margin between the tolerable upper intake level and toxic thresholds restricts their biomedical applications due to the high risk of dose-dependent toxicity[4, 5]. In recent years, based on the nanoengineering strategy, SeNPs have gradually become an important candidate material for the development of new functional selenium supplementation preparations. With their enhanced bioavailability, favorable toxicological characteristics and excellent biological activity, they have demonstrated dual application prospects in the fields of nutritional enhancement and disease intervention[6, 7]. Nevertheless,

[#]Equally first authors
***Corresponding author**
sunying@whpu.edu.cn (Ying Sun); yiy86@whpu.edu.cn (Yang Yi);

Received 13 June 2025
Received in revised from 29 July 2025
Accepted 19 September 2025

SeNPs are typically unstable due to their high surface energy, which causes them to readily aggregate, thereby losing biological activity and even exhibiting toxicity[8]. Therefore, it is urgent to develop new functionalized template materials to enhance the stability of SeNPs, thereby overcoming the clinical application bottleneck caused by its narrow therapeutic window.

Natural polysaccharides, owing to their diverse conformations and abundant reactive hydroxyl groups, are capable of modifying the surface of SeNPs via intermolecular non-covalent interactions[9]. Thus, polysaccharides have been extensively employed as capping agents to fabricate stable polysaccharide/SeNPs, and polysaccharides modified selenium nanoparticles may serve as a promising strategy to deliver a novel Se source for nutritional and therapeutic applications.

A growing number of evidences indicate that both polysaccharides and SeNPs possess significant biological activity[10-12]. The preparation of bioactive polysaccharide-functionalized SeNPs not only enhances the stability of SeNPs but also improves their biological activity and bioavailability[6, 7]. In recent years, significant synergistic interactions and nanoparticulate effects between polysaccharides and SeNPs have been validated, and polysaccharide/SeNPs have been confirmed to exhibit diverse biological effects[5]. For instance， polysaccharide-SeNPs demonstrate promising potential in anti-inflammatory activity, showing great capacity to inhibit inflammatory responses and reduce the production of inflammatory factors. As reported, a sulfated polysaccharide-stabilized SeNPs exhibited potent anti-inflammatory activity in LPS-induced RAW264.7 macrophages. This activity was mechanistically attributed to the suppression of nitric oxide (NO) production coupled with significant downregulation of mRNA levels encoding tumor necrosis factor-alpha (TNF-α), interleukin-1β (IL-1β), and inducible nitric oxide synthase (iNOS)[13]. Ulva lactuca polysaccharide-modified SeNPs were administered as dietary supplements to acute colitis mice, and exhibited significant protective effects through alleviating macrophage infiltration and inhibited the activation of macrophage by suppressing NF-κB nuclear translocation and regulating the expression of IL-6 and TNF-α[14]. Therefore, polysaccharide/SeNPs is expected to become a safe and effective anti-inflammatory agent.

In our previous studies, lotus root polysaccharide (LR) was extracted from Nelumbo nucifera Gaertn., and it is a water-soluble polysaccharide characterized as a low-molecular-weight α-1,4/6-glucan. Our researches have demonstrated its notable antioxidant, immunomodulatory, and hypolipidemic activities[15-17]. Considering its multiple bioactivities, LR is expected to be a stabilizer of SeNPs, aiming to enhance the stability and biological activity of SeNPs. Therefore, this study utilized LR as a stabilizer to synthesize a novel lotus root polysaccharide-stabilized selenium nanoparticle composite (LR/SeNPs). The physicochemical properties of LR/SeNPs, including particle size, zeta-potential, morphology, and structural characteristics, were systematically characterized. The stability and in vitro digestion behavior of LR/SeNPs under varying conditions were evaluated. Furthermore, the anti-inflammatory activity of LR/SeNPs was evaluated in macrophage to elucidate their potential therapeutic application.

2. Materials and methods

2.1. Materials and chemicals

Lotus root was supplied by Wuhan Jinshui Qiliang Agricultural By-products Company (China). Sodium chloride (NaCl), ascorbic acid (Vc) and sodium selenite (Na_2SeO_3) were obtained from National Pharmaceutical Group Corporation (China). Artificial gastric juice and small intestinal fluid were provided by Beijing Regan Biotechnology Co., LTD (China). DMEM medium and PBS were procured from Hyclone Company (USA). Lipopolysaccharide (LPS) from *E. coli* O55:B5 was acquired from MedChemExpress Company (China). Griess reagent was purchased from Nanjing Jiancheng Biological Co., LTD (China). CCK-8 reagent was obtained from Beijing Dakewe Biotech Company (China). Trizol reagent for isolation of mRNA was obtained from Wuhan Servicebio Co., LTD (China). The anti-CD86-PE and anti-CD206-FITC antibodies were procured from BioLegend Co., LTD (USA).

2.2. Extraction of lotus root polysaccharide

The lotus root polysaccharide (LR) was extracted with an amylase-assisted extraction method according to our previous work[17]. The total carbohydrate content was determined using the phenol-sulfuric acid colorimetric method according to the standardized protocol[18].

2.3. Synthesis and characterization of LR/SeNPs

LR/SeNPs were synthesized by the Na_2SeO_3/Vc reduction method, based on the previously reported protocol with minor modification[19]. In brief, 20 mmol/L Na_2SeO_3 solutions with different volumes were added to LR solutions (2 mg/mL) controlling the mass ratio of LR to Na_2SeO_3 to be 1:0.1, 1:0.2, 1:0.3, 1:0.4, and 1:0.5. And Vc solution was added in advance with the molar ratio of Vc and Na_2SeO_3 maintaining at 4:1 to ensure that Na_2SeO_3 was reduced completely. Then the systems were made up with distilled water until the concentration of LR dropped to 1.0 mg/mL. Then the products were dialyzed (MWCO, 1000 Da) with pure water for 2 days to eliminate unreacted Vc and Na_2SeO_3. The resulted solutions were named as LR/SeNPs1, LR/SeNPs2, LR/SeNPs3, LR/SeNPs4 and LR/SeNPs5. Additionally, SeNPs without LR was synthesized under the same condition as a control.

The Se contents of LR/SeNPs were measured by inductively coupled plasma-mass spectrometer (ICP-MS, NexION 350X, USA) according to the reported method[20]. The particle sizes, polydispersity indexes (PDI) and zeta-potentials of LR/SeNPs samples were evaluated with a laser granularity instrument (Malvern Instruments, UK). The incident angle was set at 90° and the refractive index of the solvent was set to 1.33. Each sample was measured three times repeatedly. The morphologies of LR/SeNPs were visualized via scanning electron microscope (SEM, Zeiss Gemini-300, Germany) and transmission electron microscope (TEM, JEOL-F200, Japan). And the surface elemental mapping and composition analysis of LR/SeNPs3 were observed via TEM and SEM equipped with EDX respectively. The FT-IR spectra of LR/SeNPs samples were recorded, with the frequency ranging from 400 to 4000 cm^{-1} (Thermo Scientific Nicolet IS20, USA). The XRD patterns of LR/SeNPs were analyzed via a powder diffractometer (Bruker AXS, USA) with the scanning range from 3° to 90° at an interval of 0.02° and a speed of 0.5° min^{-1}. The elemental composition and valence state of

Se in LR/SeNPs3 were analyzed via X-ray photoelectron spectrum (XPS, Thermo Fisher Scientific K-Alpha, USA), with LR serving as the control group.

2.4. Stability measurement of LR/SeNPs

The stability of LR/SeNPs during the storage period was assessed by laser particle size analyzer after being stored in dark at room temperature for 5, 15 and 30 days, respectively. Meanwhile, the state of the LR/SeNPs solutions were pictured and recorded.

To investigate the impact of temperature on the stability of LR/SeNPs, the temperature of LR/SeNPs3 solutions were set to 4, 37, 50 and 65 ℃ respectively, and incubated for 2 h. The changes of particle sizes and zeta-potentials were then determined using laser particle size analyzer. To measure the effect of pH, NaCl and PBS to the stability of LR/SeNPs, the buffer with different pH or NaCl and PBS with different ionic strength were prepared. For pH stability, the pH of the LR/SeNPs3 solutions (1.0 mg/mL) was adjusted by 0.1 M HCl and NaOH to be 2, 4, 6, 8 and 10, respectively. After stabilizing for 2 h, the particle sizes and zeta-potentials were detected. For the stability under different ionic strength (NaCl and PBS), 2.0 mL of NaCl solutions (5, 10, 100, 1000 mmol/L) or PBS solutions (0.01×, 0.1×, 1×, 10×, 50×) were mixed with LR/SeNPs3 solutions (1 ml, 1.0 mg/mL) respectively, then the particle sizes and zeta-potentials were determined.

2.5. In vitro simulated gastrointestinal release of LR/SeNPs

The release characteristic of LR/SeNPs was evaluated using a three-phase in vitro digestion model simulating gastrointestinal conditions. Oral phase: 2.0 mL LR/SeNPs3 solution (1.0 mg/mL) was mixed with α-amylase (2.0 mg, with an activity of 3.34×10^{-5} kat/mL) and incubated at 37 ℃ for 10 mins; Gastric phase: the oral digest was transferred into 45 mL simulated gastric liquid (SGL) containing 0.1% (w/v) pepsin. The pH was adjusted to 1.5 with 0.1 M HCl, followed by incubation in a thermostatic shaker (DHSI-II, 160 r/min) at 37℃ for 2 h; Intestinal phase: post-gastric digestion sample was centrifuged at 11,000 r/min for 30 min. The pellets were collected and resuspended in 45 mL simulated intestinal liquid (SIL) containing 1.0% (w/v) trypsin. Then the pH was adjusted to 7.4 with 1 M NaOH, and the mixture was incubated at 37℃ (120 r/min, 6 h). The digestive samples at different time points (SGL: 0, 10, 20, 30, 60, 90, 120 min; SIL: 0, 30, 60, 120, 180, 240, 300 min) were collected and named as S0, S10, S20, S30, S60, S90, S120, I0, I30, I60, I120, I180, I240 and I300 respectively. The microscopic morphologies, particle sizes and zeta-potentials of LR/SeNPs3 after digestion were observed by TEM and measured by laser particle size analyzer. Besides, the samples were centrifuged at 11000 r/min for 15 min to remove the large particles and measure the release rate of Se in LR/SeNPs3 during the digestive test. The Se concentration was quantified by ICP-MS.

The release rate of Se was calculated using the following formula:

Release rate (%) = (Mr/Mt) × 100%

where Mr represents the concentration of selenium in the digestive supernatant; Mt corresponds to the total amount of selenium.

2.6. Cell experiments

2.6.1. Cell culture and proliferation test

RAW264.7 murine macrophages (Ningbo Mingzhou Biotechnology Co., Ltd.) were maintained in Dulbecco's Modified Eagle Medium (DMEM; high glucose) supplemented with 10% (v/v) heat-inactivated fetal bovine serum (FBS), 100 U/mL penicillin and 100 μg/mL streptomycin. Cell cultures were incubated under standard physiological conditions (37℃, 5% CO_2, 95% humidity).

The proliferation effects of LR, SeNPs and LR/SeNPs3 on RAW264.7 cells were assessed via cell counting kit-8 (CCK-8) assay. In brief, cells were seeded in 96-well plates at a density of 5×10^4 cells/well and allowed to adhere for 24 h. Following treatment with serial concentrations (10-200 μg/mL) of test compounds for 24 h, 10 μL CCK-8 reagent was added to each well and incubated for 4 h at 37℃. The OD values were quantified at 450 nm using a multimode microplate reader, with 600 nm as reference wavelength.

2.6.2. Determination of NO

RAW264.7 cells were seeded in 48-well plates at a density of 2×10^5 cells/mL. Following 24 h of adhesion, the culture medium was replaced with serum-free DMEM. Cells were then treated with LR, SeNPs, or LR/SeNPs3 (10-200 μg/mL) in the presence or absence of LPS (500 ng/mL) for designated stimulation periods (24/48 h). The NO levels in the culture supernatants were quantified using the Griess reagent according to the specification. The details are provided in the supplementary materials.

2.6.3. RT-PCR assay

Total RNA was isolated from RAW264.7 macrophages treated with LR, SeNPs, or LR/SeNPs3 (100 μg/mL) under LPS-stimulated (500 ng/mL) or unstimulated conditions using TRIzol reagent (Invitrogen) according to the manufacturer's protocol. RNA integrity was verified by A260/A280 ratio (1.8~2.0) measured with a NanoDrop 2000 spectrophotometer (Thermo Fisher Scientific). Reverse transcription was performed with a PrimeScript™ RT Reagent Kit (Takara Bio) to synthesize cDNA. Quantitative real-time PCR (qRT-PCR) analysis was conducted on a LightCycler 480 system (Roche Diagnostics) with TB Green Premix Ex Taq II (Takara Bio) to quantify mRNA expression levels of iNOS, IL-1β, IL-6, TNF-α, IL-10, TGF-β1, and Arg-1, with β-actin as the endogenous control, following the method described in previous studies[21]. Primer sequences are listed in Table S1. The PCR procedure was as follows: initial denaturation at 95 ℃ for 5 min, followed by 40 cycles of amplification with denaturation at 95 ℃ for 15 seconds, annealing at 55 ℃ for 30 seconds, and extension at 72 ℃ for 30 seconds. The reaction concluded with a melting curve analysis, starting with a hold at 95 ℃ for 15 seconds, cooling to 60 ℃ for 1 min, and a final hold at 95 ℃ for 15 seconds. The resulting mRNA was normalized by β-actin mRNA and compared with the control group.

2.6.4. Immunofluorescence staining assay

To assess the impact of LR/SeNPs3 on macrophage phenotype polarization, RAW264.7 cells were seeded into 6-well plates and incubated overnight. The cells were treated by LR, SeNPs or LR/SeNPs3 (100 μg/mL) with PBS and LPS as the blank and positive controls. Following the removal of the supernatant, the cells were fixed with 4% paraformaldehyde for 15 min at room temperature. Non-specific binding sites were blocked with 5% BSA in PBS for 1 h. Fixed cells were subsequently then immunostained with fluorochrome-conjugated antibodies (anti-CD86-PE and anti-CD206-FITC, markers for M1 and M2 macrophage respectively) at 4 ℃ for 4 h in the dark. Following two washes with cold PBS, nuclei were counterstained with DAPI (1 μg/mL) for 5 min and washed twice with PBS. The fluorescent images were pictured with a confocal microscopy (LSM900, Zeiss, Germany).

2.7 Data analysis

All experimental data are presented as mean ± standard deviation (SD) from a minimum of three independent experiments. Statistical analyses were performed using SPSS 26.0 (IBM Corp.), with between-group comparisons conducted via Student's t-test and multi-group comparisons assessed by one-way ANOVA followed by Dunn’s post hoc test where appropriate. Pre-tests for the assumptions of normality and homogeneity of variance were assessed with Shapiro-Wilk test and Levene’s test respectively.

3. Results and discussion

3.1. Preparation and characterization of LR/SeNPs

Our previous research has proved that lotus root polysaccharides (LR) have good hydrophilicity and biological activity[15, 16]. To enhance the stability and biological activity of SeNPs, LR was served as stabilizer to prevent aggregation and enhance the efficacy of SeNPs. LR/SeNPs were synthesized by chemically reducing Na_2SeO_3 with Vc in LR solutions, and different mass ratios of LR:Na_2SeO_3 (1:0.1, 1:0.2, 1:0.3, 1:0.4, and 1:0.5) were designed to prepare LR/SeNPs with different Se content to optimize stability and uniformity. During the preparation of LR/SeNPs, LR and Vc were thoroughly mixed. As the Na_2SeO_3 solution was added, the color of solution gradually shifted from colorless to pale yellow and subsequently to brick red, suggesting the formation of amorphous or monoclinic selenium particles during this process. With the proportion of Na_2SeO_3 increasing from 0.1 to 0.5, the color of solution gradually darkened (Fig. 1A), suggesting that the content of SeNPs increased with the increase of Na_2SeO_3 dosage. In contrast, the SeNPs without LR showed obvious aggregation and precipitation within 24 h after preparation, indicating that LR could effectively stabilize SeNPs. The Se content and loading rate of the LR/SeNPs samples were determined by ICP-MS, and the results are presented in Fig. 1B. As the dosage of Na_2SeO_3 increased from 0.1 to 0.5, the loading amounts were 3.16%, 6.67%, 8.26%, 11.51% and 14.99%, respectively, and the loading rates of LR/SeNPs samples were around 40% without significant difference. The results of particle size and zeta-potential analysis (Fig. 1C-D) demonstrated that the average sizes of the LR/SeNPs samples were approximately 100 nm, and the size slightly increased as the Se content increasing, but it was still significantly lower than that of SeNPs (about 4251 nm). Additionally, the absolute values of

the zeta-potentials of LR/SeNPs samples were lower than that of SeNPs, illustrating that LR was attached to the surface of SeNPs. These results indicate that LR inhibited the aggregation of SeNPs effectively by modifying their surfaces.

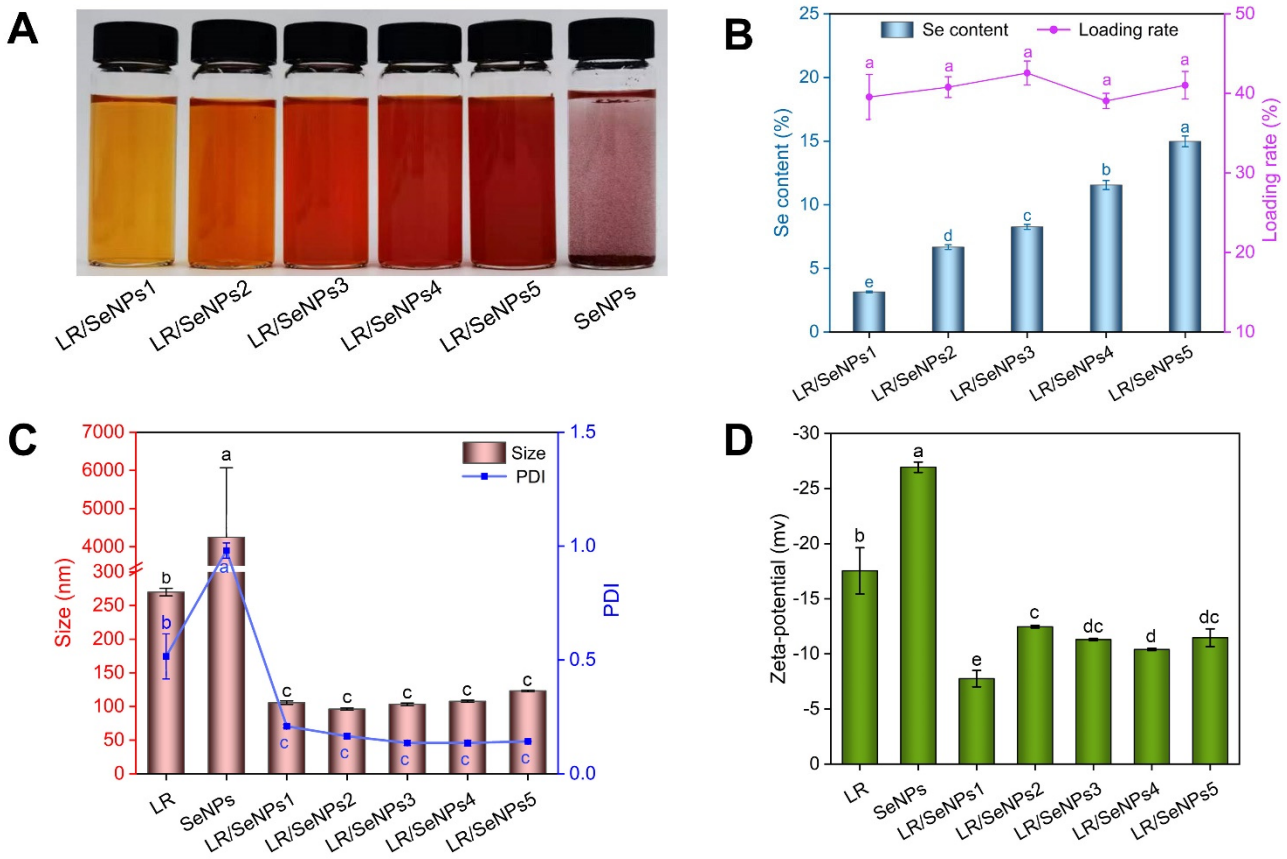

Fig. 1. The optical photograph of LR/SeNPs and SeNPs (A), the Se content and loading rate of LR/SeNPs (B), particle size (C) and zeta-potential (D) analysis of LR, SeNPs and LR/SeNPs. The data are presented as the means ± SD (n = 3). Different letters indicate significant differences ($P < 0.05$) among different groups.

Multiple characterization techniques were used to confirm the successful encapsulation and to evaluate the impact of LR on the stability, morphology and elemental distribution of SeNPs as well as the interaction between them. As shown in Fig. 2A-B, both SEM and TEM images showed that single SeNPs exhibited irregular morphologies, rough surfaces, and partial aggregation, suggesting poor dispersibility. On the contrary, LR/SeNPs samples displayed uniform spherical morphologies with smooth surfaces and negligible aggregation. This confirmed the effective encapsulation and stabilization of LR on SeNPs, which aligned with the particle size analysis results. Taking LR/SeNPs3 as the representative sample, the elemental composition of LR/SeNPs was measured by TEM mapping (Fig. 2C), revealing uniform distribution of carbon (C) and oxygen (O) throughout the particles, with Se concentrated in the core. This suggested that SeNPs was effectively encapsulated in LR, forming a stable surface layer that improved their dispersibility. Fig. 2D presents the results of SEM-EDX analysis. The surface sites of LR/SeNPs3 were selected randomly, and three elements C, O, and Se were detected and the proportions of them were 45.3 %, 11.95 %, and 42.75 % respectively. The Se content of LR/SeNPs3 was inconsistent with the result measured by ICP-MS,

which might be caused by the uneven distribution of LR and Se. In fact, LR was located on the surface of the particles, while Se was concentrated inside the particles.

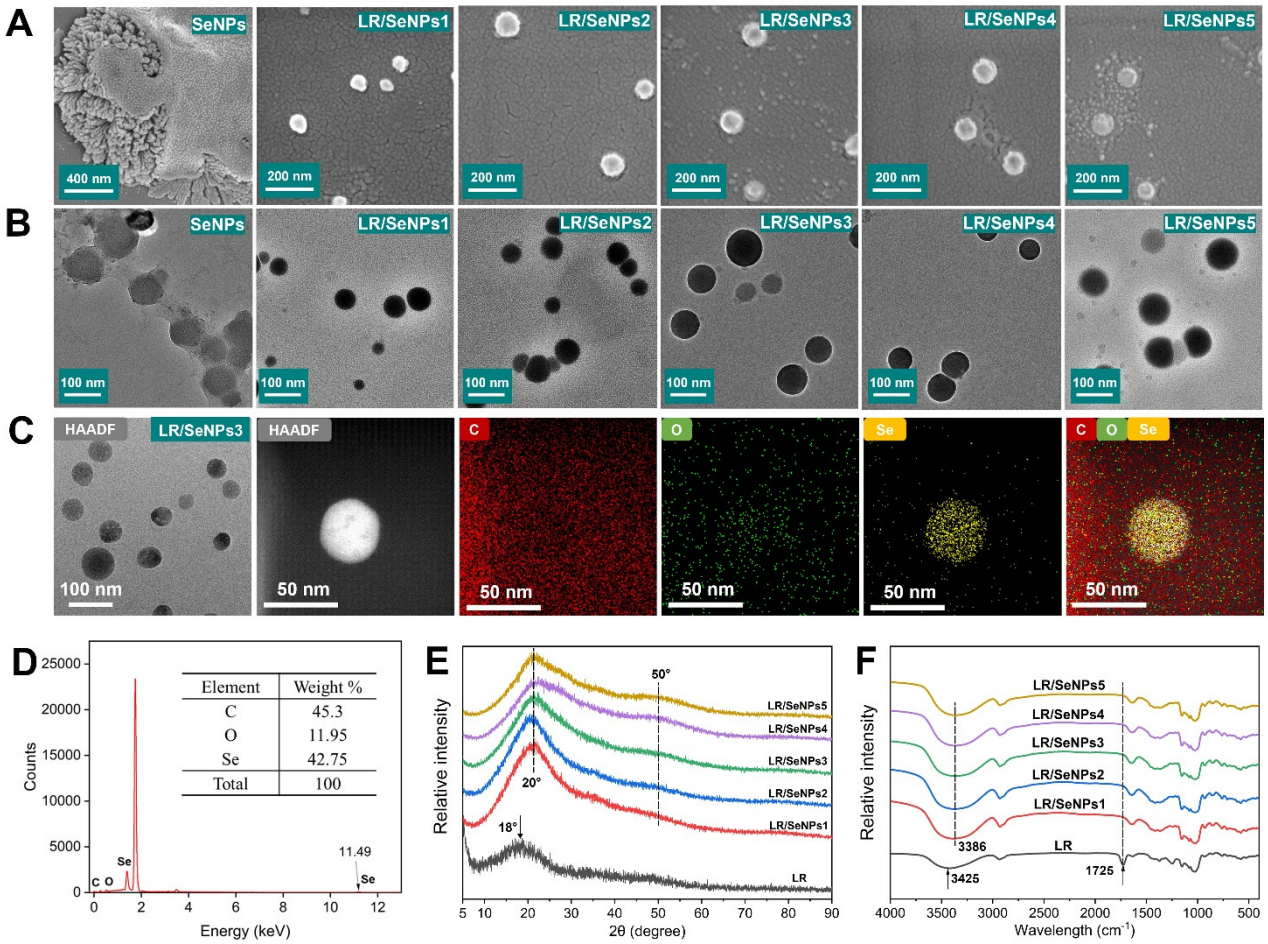

Fig. 2. Characterization of LR/SeNPs. SEM (A) and TEM (B) images of SeNPs and LR/SeNPs, the scale bar of 400 nm, 200 nm or 50 nm was marked in the lower left corner of the picture. TEM mapping (C) of LR/SeNPs3, the scale bar of 100 nm or 50 nm was marked in the lower left corner of the picture. SEM-EDX analysis (D) of LR/SeNPs3. XRD spectra (E) and FT-IR spectra (F) of LR/SeNPs.

XRD analysis was performed to characterize the crystalline phase of the prepared LR/SeNPs. As can be seen in Fig. 2E, LR exhibited sharp peaks at approximately 18° and broad reflection peaks in the range of 30°-80°, which are the typical XRD patterns of glucan[19]. In LR/SeNPs samples, the sharp peak of LR at 18° shifted to the right about 20°, This indicates that the interplanar distance of the LR crystal decreased, mainly due to the incorporation of Se atoms, which caused the distortion of the surrounding lattice[22]. In addition, compared with LR, LR/SeNPs samples showed relatively low peaks at 50° in the XRD patterns, which originated from the introduction of SeNPs and were consistent with previous reports[23]. The XRD patterns of LR/SeNPs showed no sharp peaks at 24° and 30°, which are typical of crystalline Se. Instead, there were broad, amorphous peaks, indicating that the amorphous structure of SeNPs in LR/SeNPs.

The interaction mechanism between LR and SeNPs was validated by FT-IR and XPS spectrum. In Fig. 2F, compared with LR, the characteristic absorption peak of the -OH group in LR/SeNPs shifted significantly from 3425 cm^{-1} to 3386 cm^{-1}, indicating the O-H···Se interaction between the LR and SeNPs during the formation of the LR/SeNPs. Meanwhile, it is notable that LR exhibited a distinct vibration

absorption peak for C=O at 1725 cm^{-1}, which was not present in LR/SeNPs. As reported in previous findings[24], it can be inferred that the C=O in LR was broken and the C–O···Se bond was newly formed after integrating with SeNPs. In XPS spectra (Fig. 3A), a distinct and intensified Se 3d peak emerged at 56.1 eV in LR/SeNPs, confirming successful selenium incorporation. High-resolution deconvolution of the Se 3d region (Fig. 3B) revealed two characteristic binding energies at 55.1 eV (Se^0 $3d_{3/2}$) and 54.0 eV (Se^0 $3d_{5/2}$), demonstrating complete reduction of Se^{4+} to elemental selenium (Se^0). Comparative analysis of C1s spectra (Fig. 3C-D) showed nearly identical profiles between LR and LR/SeNPs samples, indicating no detectable involvement of carbon atoms in interfacial chemical bonding. It is worth noting that there are differences in the O1s spectra of LR and LR/SeNPs (Fig. 3E-F), specifically, the O 1s absorption peaks of LR/SeNPs at 532.7 eV and 529.6 eV exhibited higher binding energies compared to those of LR at 532.3 eV and 529.2 eV, suggesting the formation of C–O···Se bonds, which was consistent with the result of the disappearance of the C=O peak as confirmed by FTIR. The bond formation induced electron density depletion around oxygen atoms, reducing their shielding efficiency toward core electrons and thereby enhancing the characteristic binding energy shift[25, 26]. In conclusion, the synthesis mechanism of LR/SeNPs involves two sequential steps: initially, selenite ions (SeO_3^{2-}) are reduced to elemental selenium (Se^0) by Vc; subsequently, the nascent Se^0 nuclei are stabilized through interfacial interactions with LR, forming C-O···Se coordination bonds and hydrogen-bond networks, thus preventing the aggregation of SeNPs and facilitating the formation of well-dispersible LR/SeNPs.

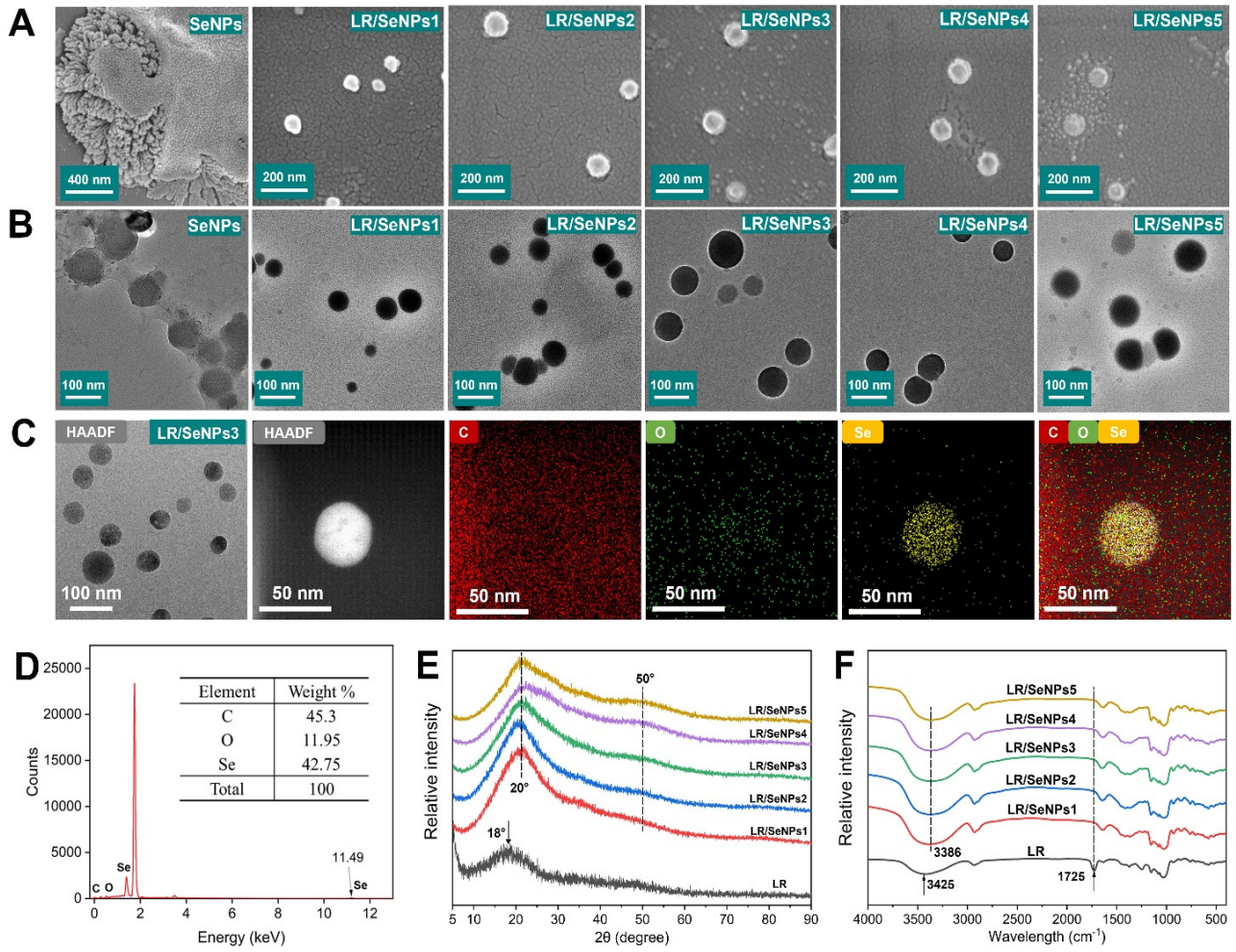

Fig. 3. X-ray photoelectron spectroscopy (XPS) of LR and LR/SeNPs3.

3.2. Stability of LR/SeNPs.

Stability is a critical factor influencing the bioactivity and application of SeNPs. Fig. 4A displayed the storage stability of LR/SeNPs. It can be seen that the SeNPs alone showed obvious aggregation and precipitation after preparation, while the stability is significantly improved by coating LR. With the increase of storage time from day 0 to day 30, the stability of LR/SeNPs samples showed differences. Among them, the appearance of LR/SeNPs2, LR/SeNPs3 and LR/SeNPs4 remained basically unchanged during the 30-day storage process, while the color of LR/SeNPs1 turned black at day 30, which may be due to the oxidation of SeNPs. The uniformity of LR/SeNPs5 did not change much within 15 days of storage, but obvious stratification appeared at day 30, which might be due to the sedimentation of solid substances caused by the excessively high concentration of the system. Meanwhile, we monitored the particle sizes and zeta-potentials of the LR/SeNPs at 0, 5, 15 and 30 days (Fig. 4B-C). The particle size of the LR/SeNPs samples remained unchanged during the 5-day storage period. However, on the 15th and 30th days, the particle sizes of LR/SeNPs1 and LR/SeNPs2 increased significantly, while the sizes of LR/SeNPs3, LR/SeNPs4 and LR/SeNPs5 changed little. The similar trend was also observed in zeta-potential, indicating that LR/SeNPs3, LR/SeNPs4 and LR/SeNPs5 had good storage stability. In order to compare the characteristics of the LR/SeNPs samples visually, we summarized the key properties of LR/SeNPs1-5,

including loading capacity, particle size, zeta potential and stability result (Table S2). We can find that both LR/SeNPs2 and LR/SeNPs4 showed good storage stability but the loading rate was lower than that of LR/SeNPs3. And LR/SeNPs5 exhibited a layering phenomenon after storage for 30 days due to the imbalance of molecular forces. Among LR/SeNPs samples, LR/SeNPs3 maintained stable particle size and zeta potential within 30 days, without stratification or oxidation, and had the highest loading rate. Therefore, we chose LR/SeNPs3 for the subsequent experimental research.

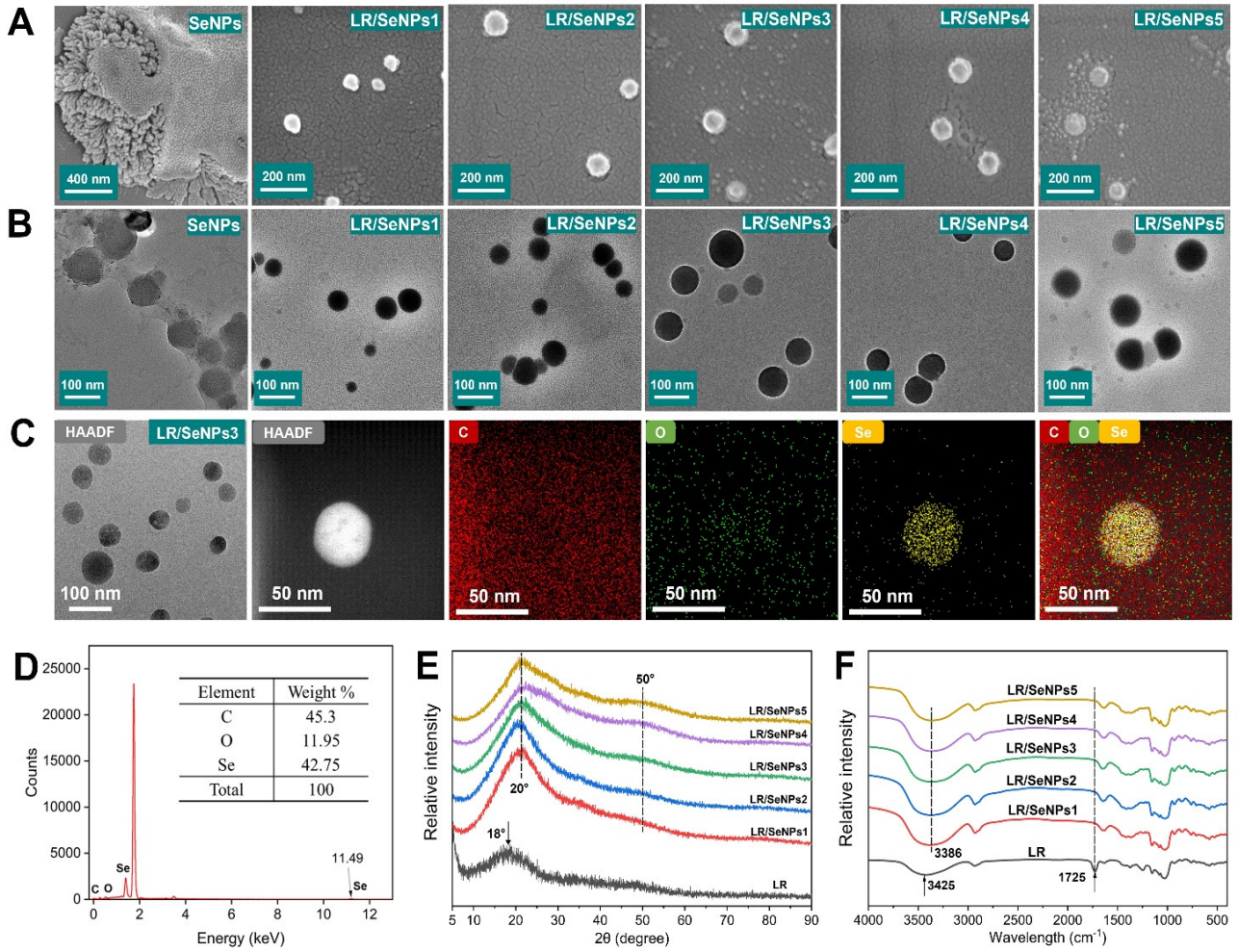

Fig. 4. The photographs (A), particle sizes (B) and zeta-potentials (C) analysis of LR/SeNP and SeNPs stored in dark at room temperature for 0, 5, 15, and 30 days. The data are presented as the means ± SD (n = 3), $^{*}p<0.05$ indicates significant differences between two groups and ns indicates no significant difference between two groups.

In order to verify the stability and effectiveness of LR/SeNPs3 in practical applications, its performance under various environmental conditions was tested. The stability of LR/SeNPs3 was investigated under different temperature (4 ℃, 25 ℃, 37 ℃, 50 ℃, 65 ℃), different pH (2, 4, 6, 8, 10) and two common solvents: NaCl solution (5, 10, 100, 1000 mmol/L) and PBS buffer (0.01×, 0.1×, 1×, 10×, 50×). As shown in Fig. 5A-B, within the range of 4~50 ℃, the particle size of LR/SeNPs3 changed little, and the absolute value of zeta-potential slightly reduced compared with that at 4 ℃, manifesting good stability at 4~50 ℃. While at 65 ℃, the particle size and zeta-potential changed significantly, which indicated that the temperature exceeding 65 ℃ would undermine the stability of LR/SeNPs3. The pH stability results (Fig. 5C-D) show that LR/SeNPs3 was unstable in acidic environments (pH 2 to 4), exhibiting significant increase

in size and decrease in zeta-potential compared to the control group. In contrast, under neutral, slightly acidic or slightly alkaline conditions (pH 6, 8, 10), the particle sizes maintained between 145 nm and 150 nm, and the zeta-potential was between -11 mV and -12 mV, indicating better stability. This indicated that extreme acidic pH diminished stability by reducing electrostatic repulsion. In NaCl solution with different concentrations (Fig. 5E-F), the size of LR/SeNPs3 increased from 150 nm to 270 nm with the NaCl concentration increasing from 0 to 1000 mmol/L, meanwhile, the absolute value of the zeta-potential decreased in a concentration-dependent manner. This situation might be due to the fact that the Na^+ adsorb onto the surface of LR/SeNPs, neutralizing the negative charges on its surface and reducing the absolute value of the zeta-potential, thereby causing aggregation. Meanwhile, salt ions also shielded the interaction between the active sites on the LR chain and SeNPs, leading to a decrease in the stability of the coating layer and easy aggregation of particles, which was manifested as an increase in particle size with the rise of NaCl concentration. Similar phenomena were also observed in different concentrations of PBS solution (Fig. 5G-H). With the increase of PBS concentration, the net charge of LR/SeNPs3 decreased obviously, nevertheless, within the concentration range of 0.01 to 10×, no significant difference was observed between LR/SeNPs3 and the control group in particle size. This might be due to the strong buffering effect of PBS. The ionic strength of PBS at low to medium concentrations has not yet exceeded the steric hindrance stability threshold of the LR coating layer. In the PBS system, the phosphate ions with a larger size formed coordination bonds with the LR polysaccharide chains, creating spatial hindrance, which could partially counteract the particle aggregation caused by the decrease in zeta-potential value. According to the DLVO theory, this phenomenon can be explained as that the low pH and high ionic strength environment compressed the double electric layer on the surface of LR/SeNPs3 through electrostatic neutralization and salt shielding, reduced the electrostatic repulsion and enhanced the van der Waals force, thereby leading to particle aggregation. Therefore, to mitigate aggregation and maintain long-term stability, the storage of LR/SeNPs should be prevented from high temperatures, high acidity and high salt environments.

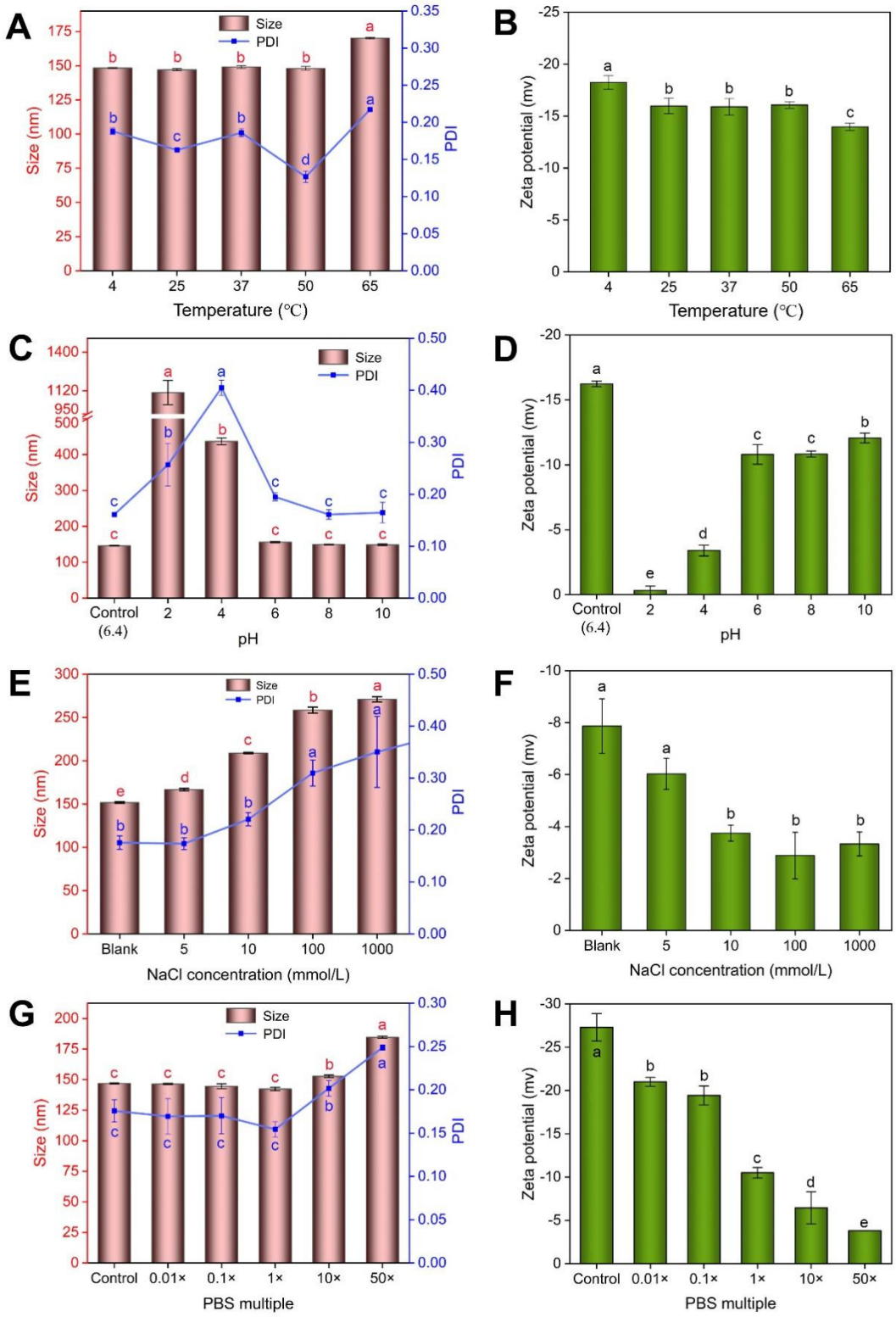

Fig. 5. Particle sizes and zeta-potentials of LR/SeNPs3 under different temperature (A, B), different pH (C, D), NaCl (E, F) and PBS (G, H) with different concentration. The data are presented as the means ± SD (n = 3). Different letters indicate significant differences ($P < 0.05$) among different groups.

3.3. In vitro simulated gastrointestinal release of LR/SeNPs

The recommended daily intake of selenium for adults ranges from 55 to 400 μg, indicating the narrow margin between nutritional and toxic doses[27]. Therefore, the analysis of release characteristics of SeNPs is crucial for their application in dietary supplements, considering the different gastrointestinal environments.

Fig. 6A illustrated the release profiles of LR/SeNPs3 during digestion in simulated gastric fluid (SGF, pH 1.2) and simulated intestinal fluid (SIF, pH 7.4). The results demonstrated a time-dependent release pattern. The fast release of Se was observed in SGL digestion, due to the strong acid and pepsin in SGL, which caused the partial degradation and relaxation of LR, resulting in the exposure of the inner layer of SeNPs. During the simulated intestinal digestion stage, the release of Se slowed down. In an environment close to neutral pH, LR/SeNPs3 remained relatively stable, and the trypsin in SIL catalyzed and hydrolyzed the LR on the surface, enabling the continuous slow release of Se. The maximum Se release rate of LR/SeNPs3 throughout the digestion process was 12.27%, which suggested sustained stability of LR/SeNPs3 and could be uptake as intact nanoparticles. This is mainly because the high surface energy of SeNPs itself and the continuous adsorption of LR residues jointly limit the rapid dissociation of selenium atoms. The release profile indicated that the SeNPs encapsulated with LR polysaccharides have a stable structure and a high intestinal retention rate, which can prevent excessive selenium release and reduce the risk of toxicity. However, this did not imply a low biological utilization rate. This long-lasting release characteristic would become more crucial when the LR/SeNPs3 pass through the intestinal tract and enter the body's circulation, which could maintain the selenium homeostasis in the body and avoid toxicity. Similar release trends have also been reported in the previous study. Zhang et al used Lycium barbarum polysaccharides to stabilize selenium nanoparticles, and the maximum release rate was approximately 12.11%[28]. Guo et al reported that the total release amount of selenium nanoparticles stabilized by Lycium barbarum polysaccharide-protein was 9%[29]. This slow release can reduce the risk of acute Se exposure, which meets the requirements of long-acting and low toxicity for dietary supplements. The results demonstrated that the LR/SeNPs3 showed great stability under strong acid and enzymatic conditions and LR exerted a crucial protective effect on SeNPs.

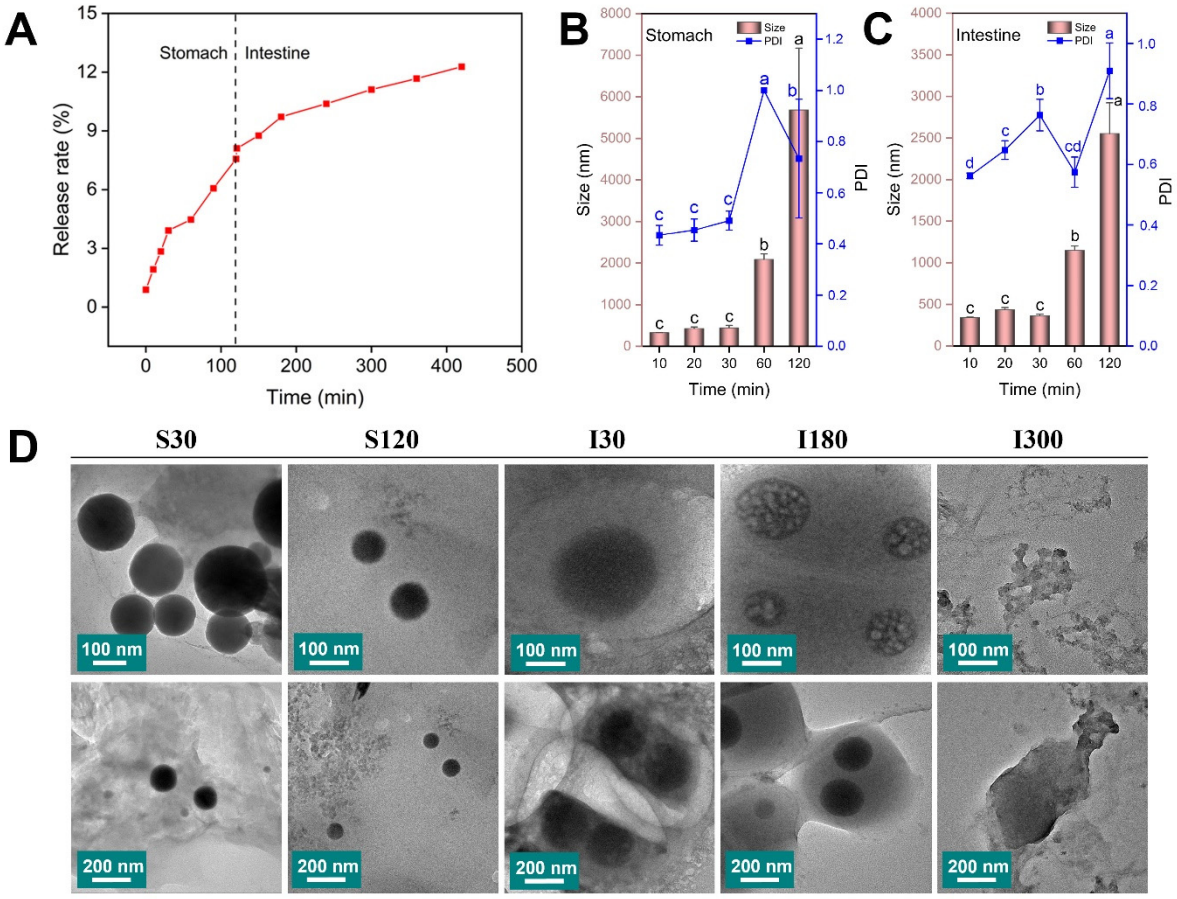

Fig. 6. In vitro release rate of LR/SeNPs3 in the simulated gastric and intestinal conditions (A). Particle size and PDI of LR/SeNPs3 at different digestion time points (B, C). TEM images of LR/SeNPs3 during the simulated digestion at different time points (D). The data are presented as the means ± SD (n = 3). Different letters indicate significant differences ($P < 0.05$) among different groups.

The pH changes and the proteolytic enzymes in gastrointestinal fluid significantly influence the particle size and structural integrity of SeNPs. As shown in Fig. 6B-C, compared with the initial state, the particle size of LR/SeNPs3 exhibited a significant increase ($p<0.05$) after being exposed to SGL digestion for 120 min, which has been verified in the previous pH stability test. When LR/SeNPs3 entered the intestinal tract, the particle size returned to its initial nanoscale. This phenomenon indicated that LR/SeNPs3 could resist the damage caused by the acidic gastric environment. As the subsequent digestion progressed, the particle size gradually increased. This is due to the hydrolysis effect of enzymes, which caused the polysaccharides to detach from the surface of the SeNPs and triggered aggregation. TEM images (Fig. 6D) indicated that LR/SeNPs3 still maintained a spherical structure after being digested by SGL, and during the intestinal digestion process, the particles gradually break down, showing slow releasing characteristics, thus most LR/SeNPs3 could be absorbed within the intestinal tract.

3.4. Anti-inflammatory activity of LR/SeNPs

The SeNPs are garnering much attention due to their potential application in the treatment of various diseases, especially in some inflammation-related diseases such as rheumatoid arthritis (RA), inflammatory bowel disease (IBD) and multiple autoimmune disorders[30, 31]. Our prior research demonstrated that LR had

exhibited significant effects in immune modulation[16], thus, the anti-inflammatory activity of LR/SeNPs3 and whether LR exerted a synergistic effect were explored. The experiment was carried out in the RAW 264.7 macrophages.

The effect of LR/SeNPs3 on the viability of RAW264.7 cells was evaluated by the CCK-8 assay. As illustrated in Fig. 7A, neither LR nor LR/SeNPs3 showed significant toxicity to RAW264.7 cells. at concentration ranging from 10 to 200 μg/mL. The concentration of SeNPs was set to be equivalent to the concentration of Se in the LR/SeNPs3. It can be observed that SeNPs also showed no significant toxicity within this concentration range.

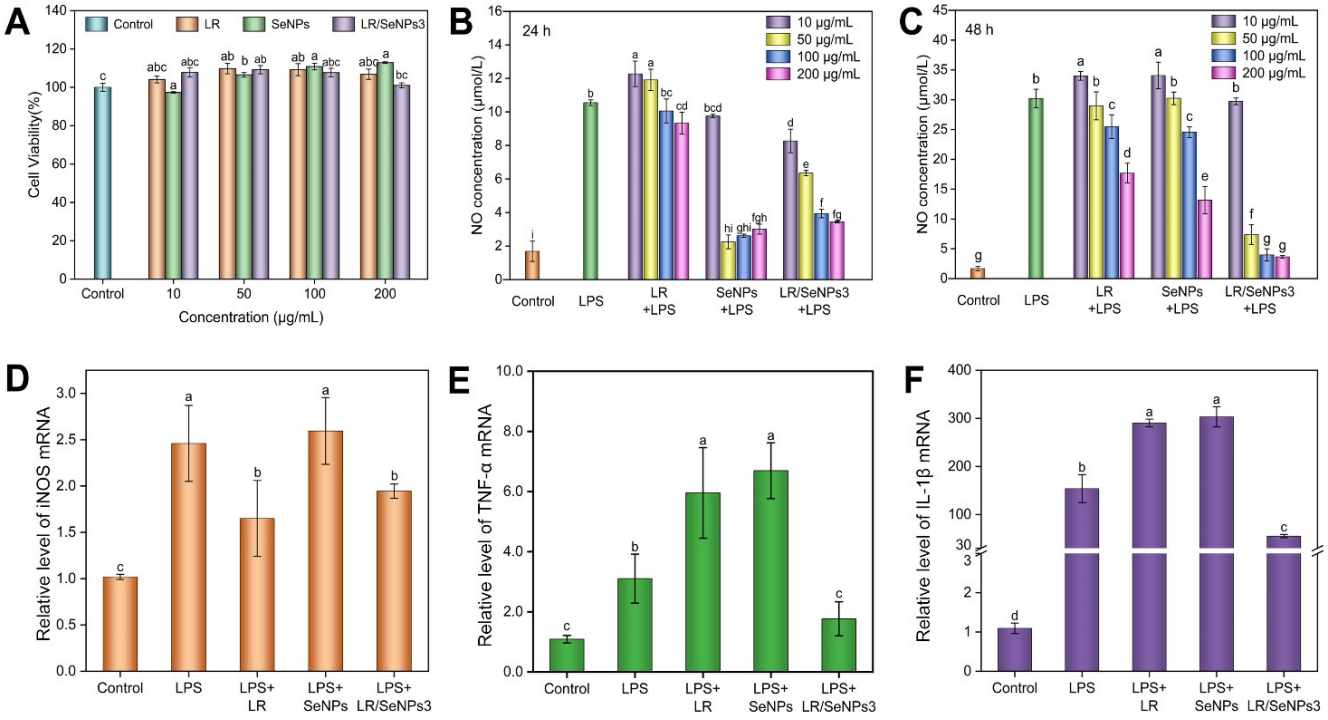

Fig. 7. The effect of LR, SeNPs and LR/SeNPs3 on the viability of RAW264.7 cells (A). Effect of LR, SeNPs and LR/SeNPs3 on NO production in LPS-induced RAW 264.7 cells at 24 h (B) and 48 h (C). Effect of LR, SeNPs and LR/SeNPs3 on the mRNA level of iNOS (D), TNF-α (E) and IL-1β (F) in LPS induced RAW 264.7 cells at 12 h. The data are presented as the means ± SD (n = 3). Different letters indicate significant differences ($P < 0.05$) among different groups. The mRNA expression levels are represented as fold changes.

To investigate the anti-inflammatory effects of LR/SeNPs3, NO levels were quantitatively assessed in LPS-stimulated RAW264.7 macrophages treated with LR, SeNPs, or LR/SeNPs3 for 24 h (Fig. 7B) and 48 h (Fig. 7C). Notably, LPS challenge significantly enhanced NO production in RAW264.7 cells compared to untreated controls. With the addition of LR, SeNPs or LR/SeNPs3, the increase in NO caused by LPS was inhibited to varying degrees. LR at 200 μg/mL showed significant inhibition of NO production at both 24 h (p = 4.1E-10 *vs.* LPS group) and 48 h (p = 3.1E-17 *vs.* LPS group), illustrating that LR had a certain anti-inflammatory activity. It is worth noting that, SeNPs in the absence of LR could inhibit the generation of NO at 24 h, but the inhibitory effect weakened as time went on to 48 h. The reason is that SeNPs tended to aggregate into larger sizes due to their higher surface energy, and had a limited contact surface with macrophages. Besides, due to the aggregation of SeNP itself, the negative charge of its surface became higher, which led to a repulsive effect with the negatively charged phospholipid bilayer of the cell

membrane, making it more difficult to be internalized by the cell. However, LR/SeNPs3 treatment markedly decreased the levels of NO from 30 to 3~7.5 μmol/L at 48 h (inhibition rate＞75%) at concentrations of 10-200 μg/mL. It was more effective than LR or SeNPs treatment alone, highlighting the ability of LR/SeNPs3 to relieve inflammatory response via the reduction of NO production. Thess results demonstrated that the combination of LR could significantly enhance the anti-inflammatory ability of SeNPs, which may be attributed to the excellent dispersion effect of LR on SeNPs, enabling them to have an increased interaction with cells. Additionally, LR alone also had a certain inhibitory effect on the increase in NO caused by LPS, and our previous work has demonstrated the antioxidant and immunomodulatory activity of LR[15, 16], which could prevent SeNPs from being oxidized and deactivated when coated on the surface of SeNPs, and show a synergistic anti-inflammatory effect, so that LR played a crucial role in the process of LR/SeNPs3 exerting anti-inflammatory activity.

During the development of inflammation, in addition to the excessive expression of NO, inflammatory factors such as TNF-α, iNOS and IL-1β are also upregulated, thereby exacerbating the inflammatory response of the body[32]. To determine whether the inhibitory effect of LR/SeNPs3 on inflammation was associated with modulation of iNOS, TNF-α, and IL-1β, the transcriptional gene expression levels of these factors in LPS-stimulated RAW264.7 cells were measured by RT-PCR (Fig. 7D-F). The results show that LR/SeNPs3 was able to significantly inhibit the upregulation of iNOS (p = 0.046 *vs.* LPS group), TNF-α (p = 0.026 *vs.* LPS group) and IL-1β (p = 0.002 *vs.* LPS group) mRNA caused by LPS, but it is noteworthy that LR and SeNPs did not exhibit significant inhibitory effects on the mRNA expression levels of these cytokines under the same experimental conditions, indicating that LR/SeNPs3 showed better anti-inflammation effect.

3.5. Macrophages phenotypic regulation of LR/SeNPs

Macrophages can be influenced by various factors and change their phenotypes, thereby affecting their functions. Activated macrophages are generally categorized into two types, designated as M1- type and M2-type macrophages. Among them, M1-type macrophages predominantly mediate pro-inflammatory responses, whereas M2-type macrophages are primarily involved in anti-inflammatory responses. Regulating the activation state of macrophages to improve the inflammatory environment is an effective method for treating diseases. The transformation of macrophages into the M2 phenotype is crucial for modulating inflammatory responses[33, 34]. To further elucidate the anti-inflammatory mechanism of LR/SeNPs3, we employed confocal laser scanning microscopy (CLSM) to observe and analyze the expression levels of CD86 (M1-type) and CD206 (M2-type) in RAW264.7 cells treated by LR/SeNPs3, with PBS and LPS serving as the negative and positive controls, respectively. As shown in Fig. 8A-B, LPS treatment markedly upregulated CD86 expression, whereas CD206 expression changed little, indicating that LPS caused M1 polarization of RAW264.7 macrophages, consisting with the reported literature[35]. By comparing the fluorescence intensities, it was found that the order of the degree for promoting the expression level of CD86 was LPS ≈ SeNPs > LR ≈ LR/SeNPs3, while the order of the expression level of

CD206 was SeNPs ≈ LPS < LR < LR/SeNPs3, illustrating that LR/SeNPs3 could promote the M2 polarization of RAW264.7 macrophages.

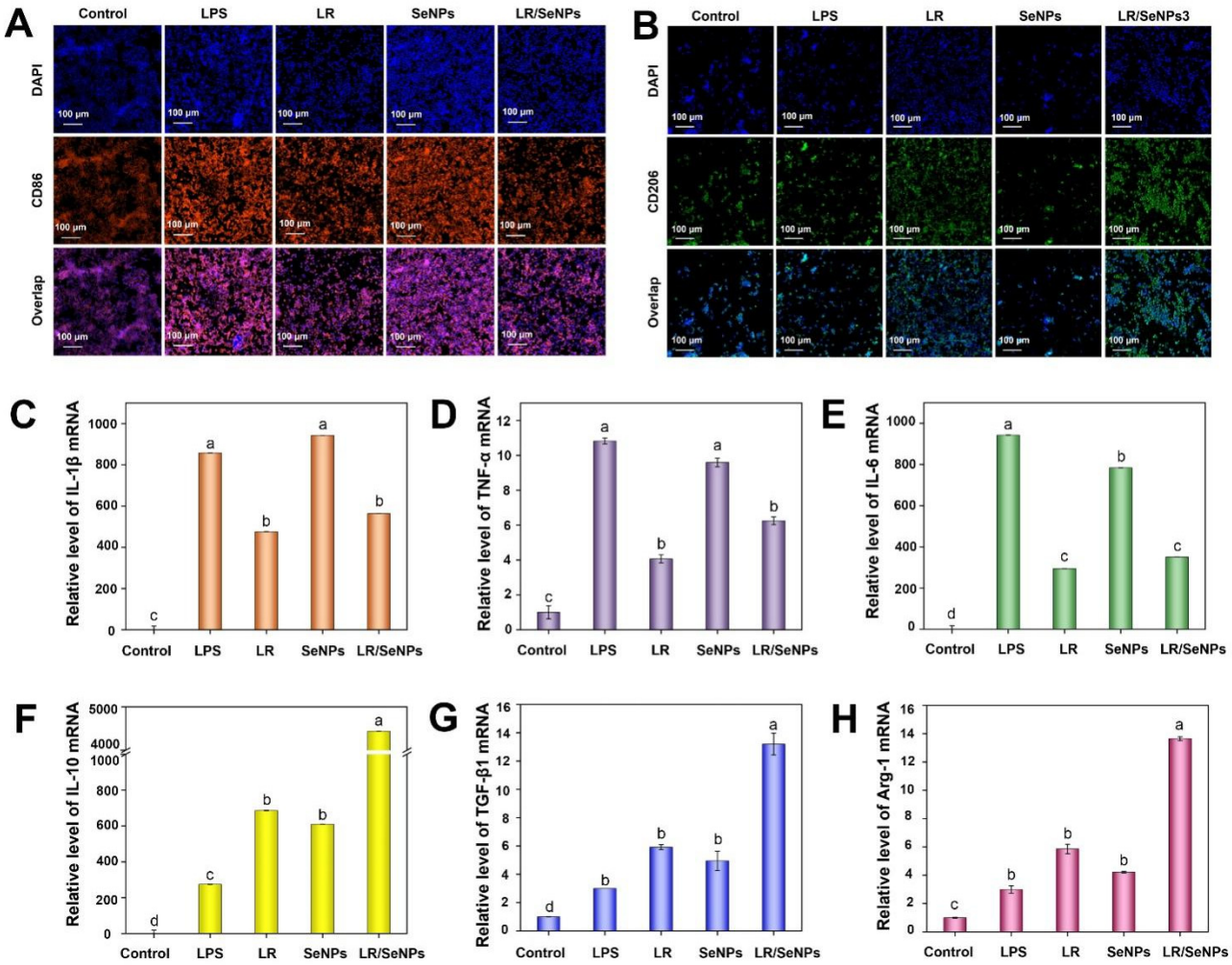

Fig. 8. Immunofluorescence examination of CD86 (red) and CD206 (green) of the RAW264.7 cells induced by LR, SeNPs and LR/SeNPs3 (A, B). Effect of LR, SeNPs and LR/SeNPs3 on the mRNA level of IL-1β (C), TNF-α (D), IL-6 (E), IL-10 (F), TGF-β1 (G) and Arg-1 (H) in RAW 264.7 cells at 12 h. The data are presented as the means ± SD (n = 3). Different letters indicate significant differences ($P < 0.05$) among different groups. mRNA expression levels are represented as fold changes.

The pivotal regulatory mechanism underlying macrophage phenotypic polarization manifests as dynamic alterations in specific cytokine expression profiles. M1-polarized macrophages are characterized by transcriptional upregulation of pro-inflammatory mediators, notably including canonical cytokines such as IL-1β, TNF-α, and IL-6. Conversely, M2-polarized macrophages, serving as molecular hallmarks of anti-inflammatory phenotypes, exhibit significant upregulation in the expression of anti-inflammatory mediators including IL-10, TGF-β1, and Arg-1[36, 37]. Thus, the mRNA levels of the characteristic factors were determined by RT-PCR. As shown in Fig. 8C-H, in contrast to LPS, LR/SeNPs3 could significantly down-regulate the RNA levels of IL-1β, TNF-α and IL-6, and up-regulate the relative levels of IL-10, TGF-β1 and Arg-1, which further proved the effect of LR/SeNPs3 in promoting M2 polarization of macrophages. Additionally, LR also promoted macrophages M2 polarization to some extent, showing a synergistic effect. While SeNPs showed no significant difference in promoting or inhibiting the expression

of these factors compared to LPS, indicating that the biological activity of un-stabilized selenium nanoparticles is difficult to be exerted. These results were consistent with the immunofluorescence data, confirming that LR/SeNPs3 exhibited a significantly enhanced regulatory effect on promoting macrophage polarization towards the anti-inflammatory M2 phenotype compared to SeNPs alone.

This study explored the synthesis and stability conditions of selenium nanoparticles stabilized by LR, as well as their *in vitro* anti-inflammatory activity. However, the *in vivo* anti-inflammatory activity of LR/SeNPs in inflammatory animal models, such as colitis models, and their detailed anti-inflammatory mechanisms need further exploration. We will conduct researches on these issues in our subsequent studies.

4. Conclusion

In summary, we successfully synthesized a series of LR/SeNPs with varying Se content using LR as the stabilizer. Systematic characterization revealed that LR surface functionalization significantly improved the stability of SeNPs. Mechanistic studies indicated that the enhanced stability of LR/SeNPs originated from the formation of C–O···Se bonds and strong hydrogen-bond interactions between LR and SeNPs. Among the LR/SeNPs samples, LR/SeNPs3, LR/SeNPs4 and LR/SeNPs5 had good storage stability during the period of 30 days with little change in sizes and zeta-potentials. Meanwhile, we illustrated that the storage of LR/SeNPs should be prevented from high temperatures, high acidity and high salt environments to mitigate aggregation and guarantee long-term stability. In simulated gastrointestinal environment, LR/SeNPs3 exhibited high retention rate in SGL and a continuous and slow-release characteristic in SIL. In addition, LR/SeNPs3 demonstrated significant anti-inflammatory effects by inhibiting NO production, downregulating mRNA expression of iNOS, TNF-α, and IL-1β, and promoting macrophage polarization toward the anti-inflammatory M2 phenotype. Our current findings provide basic insights into the role of LR/SeNPs in anti-inflammation in vitro, future in vivo studies using inflammatory disease models (e.g., colitis) are planned to validate the translational relevance of these results. Collectively, this study provided an effective way for stabilization of SeNPs, and a theoretical basis for Se supplementary strategy and nanomaterial-guided treatment of inflammatory diseases.

Declaration of competing interest

The authors declared that there is no conflict of interest.

Data availability

Data will be made available on request.

References

[1] H. Tapiero, D.M. Townsend, K.D. Tew, The antioxidant role of selenium and seleno-compounds, Biomed. Pharmacother. 57 (2003) 134-144. https://doi.org/10.1016/s0753-3322(03)00035-0.

[2] C. Sanmartin, D. Plano, A.K. Sharma, et al., Selenium compounds, apoptosis and other types of cell death: An overview for cancer therapy, Int. J. Mol. Sci. 13 (2012) 9649-9672. https://doi.org/10.3390/ijms13089649.

[3] S. Skalickova, V. Milosavljevic, K. Cihalova, et al., Selenium nanoparticles as a nutritional supplement, Nutrition. 33 (2017) 83-90. https://doi.org/10.1016/j.nut.2016.05.001.

[4] C.M. Weekley, H.H. Harris, Which form is that? The importance of selenium speciation and metabolism in the prevention and treatment of disease, Chem. Soc. Rev. 42 (2013) 8870-8894. https://doi.org/10.1039/c3cs60272a.

[5] T. Zhang, M. Qi, Q. Wu, et al., Recent research progress on the synthesis and biological effects of selenium nanoparticles, Front. Nutr. 10 (2023) 1183487. https://doi.org/10.3389/fnut.2023.1183487.

[6] A. Khurana, S. Tekula, M.A. Saifi, et al., Therapeutic applications of selenium nanoparticles, Biomed. Pharmacother. 111 (2019) 802-812. https://doi.org/10.1016/j.biopha.2018.12.146.

[7] X. Xiao, H. Deng, X. Lin, et al., Selenium nanoparticles: Properties, preparation methods, and therapeutic applications, Chem.-Biol. Interact. 378 (2023) 110483. https://doi.org/10.1016/j.cbi.2023.110483.

[8] S.A. Wadhwani, U.U. Shedbalkar, R. Singh, et al., Biogenic selenium nanoparticles: current status and future prospects, Appl. Microbiol. Biotechnol. 100 (2016) 2555-2566. https://doi.org/10.1007/s00253-016-7300-7.

[9] X.D. Shi, Y.Q. Tian, J.L. Wu, et al., Synthesis, characterization, and biological activity of selenium nanoparticles conjugated with polysaccharides, Crit. Rev. Food Sci. Nutr. 61 (2021) 2225-2236. https://doi.org/10.1080/10408398.2020.1774497.

[10] X.B. Li, F.C. Jiang, M.Y. Liu, et al., Synthesis, characterization, and bioactivities of polysaccharide metal complexes: A review, J. Agric. Food Chem. 70 (2022) 6922-6942. https://doi.org/10.1021/acs.jafc.2c01349.

[11] E.G. Varlamova, E.A. Turovsky, E.V. Blinova, Therapeutic potential and main methods of obtaining selenium nanoparticles, Int. J. Mol. Sci. 22 (2021) 10808. https://doi.org/10.3390/ijms221910808.

[12] C.Y. Hou, L.L. Chen, L.Z. Yang, et al., An insight into anti-inflammatory effects of natural polysaccharides, Int. J. Biol. Macromol. 153 (2020) 248-255. https://doi.org/10.1016/j.ijbiomac.2020.02.315.

[13] S.Q. Hu, W.C. Hu, Y.R. Li, et al., Construction and structure-activity mechanism of polysaccharide nano-selenium carrier, Carbohydr. Polym. 236 (2020) 116052. https://doi.org/10.1016/j.carbpol.2020.116052.

[14] C.H. Zhu, S.M. Zhang, C.W. Song, et al., Selenium nanoparticles decorated with Ulva lactuca polysaccharide potentially attenuate colitis by inhibiting NF-κB mediated hyper inflammation, J. Nanobiotechnol. 15 (2017) 20. https://doi.org/10.1186/s12951-017-0252-y.

[15] Y. Yi, X.Y. Huang, Z.T. Zhong, et al., Structural and biological properties of polysaccharides from lotus root, Int. J. Biol. Macromol. 130 (2019) 454-461. https://doi.org/10.1016/j.ijbiomac.2019.02.146.

[16] Y. Sun, M.J. Zhang, X.Y. Jiang, et al., Structural characterization and immunoregulatory mechanism of a low-molecular-weight polysaccharide from lotus root, Int. J. Biol. Macromol. 280 (2024) 135957. https://doi.org/10.1016/j.ijbiomac.2024.135957.

[17] J. Song, Z. Zhang, H.X. Wang, et al., Study on the structure and lipid-lowering activity of different components of lotus root polysaccharides, Food Res. Int. 203 (2025) 115801. https://doi.org/10.1016/j.foodres.2025.115801.

[18] M. DuBois, K.A. Gilles, J.K. Hamilton, et al., Colorimetric method for determination of sugars and related substances, Anal. Chem. 28 (1956) 350-356. https://doi.org/10.1021/ac60111a017.

[19] Y. Sun, L.S. Liang, Y. Yi, et al., Synthesis, characterization and anti-inflammatory activity of selenium nanoparticles stabilized by aminated yeast glucan, Int. J. Biol. Macromol. 245 (2023) 125187. https://doi.org/10.1016/j.ijbiomac.2023.125187.

[20] Y.D. Xiao, Q.L. Huang, Z.M. Zheng, et al., Selenium release kinetics and mechanism from Cordyceps sinensis exopolysaccharide-selenium composite nanoparticles in simulated gastrointestinal conditions, Food Chem. 350 (2021) 129223. https://doi.org/10.1016/j.foodchem.2021.129223.

[21] Y. Sun, X.D. Shi, X. Zheng, et al., Inhibition of dextran sodium sulfate-induced colitis in mice by baker's yeast polysaccharides, Carbohydr. Polym. 207 (2019) 371-381. https://doi.org/10.1016/j.carbpol.2018.11.087.

[22] J.Y. Qian, W. Chen, W.M. Zhang, et al., Adulteration identification of some fungal polysaccharides with SEM, XRD, IR and optical rotation: A primary approach, Carbohydr. Polym. 78 (2009) 620-625. https://doi.org/10.1016/j.carbpol.2009.05.025.

[23] X. Gao, X. Li, J. Mu, et al., Preparation, physicochemical characterization, and anti-proliferation of selenium nanoparticles stabilized by Polyporus umbellatus polysaccharide, Int. J. Biol. Macromol. 152 (2020) 605-615. https://doi.org/10.1016/j.ijbiomac.2020.02.199.

[24] Z. Yang, Y. Hu, P. Yue, et al., Structure, stability, antioxidant activity, and controlled-release of selenium nanoparticles decorated with lichenan from Usnea longissima, Carbohydr. Polym. 299 (2023) 120219. 120219. https://doi.org/10.1016/j.carbpol.2022.120219.

[25] N. Bhiri, N. Masquelez, M. Nasri, et al., Synthesis, characterization, and stability study of selenium nanoparticles coated with purified polysaccharides from ononis natrix, Nanomaterials. 15 (2025) 435. https://doi.org/10.3390/nano15060435.

[26] Z.M. Dou, Y.L. Zhang, C.Y. Tang, et al., Construction of blackberry polysaccharide nano-selenium particles: Structure features and regulation effects of glucose/lipid metabolism in HepG2 cells, Food Res. Int. 187 (2024) 114428. https://doi.org/10.1016/j.foodres.2024.114428.

[27] X. Gu, C.Q. Gao, New horizons for selenium in animal nutrition and functional foods, Anim. Nutr. 11 (2022) 80-86. https://doi.org/10.1016/j.aninu.2022.06.013.

[28] J.X. Zhang, X. Yang, T. Ji, et al., Digestion and absorption properties of Lycium barbarum polysaccharides stabilized selenium nanoparticles, Food Chem. 373 (2022) 131637. https://doi.org/10.1016/j.foodchem.2021.131637.

[29] G.Y. Liu, T. Ji, J.W. Pan, et al., Study on the digestion and absorption property of Lycium barbarum polysaccharide-protein stabilized selenium nanoparticles from the perspective of stability in vitro, Lwt-Food Sci. Technol. 198 (2024) 115921. https://doi.org/10.1016/j.lwt.2024.115921.

[30] J.A. Ansari, J.A. Malik, S. Ahmed, et al., Recent advances in the therapeutic applications of selenium nanoparticles, Mol. Biol. Rep. 51 (2024) 688. https://doi.org/10.1007/s11033-024-09598-z.

[31] D.S. Chen, H.M. Lu, Y.H. Ma, et al., Trends and recent progresses of selenium nanoparticles as novel autophagy regulators for therapeutic development, Front. Nutr. 10 (2023) 1116051. https://doi.org/10.3389/fnut.2023.1116051.

[32] E. Eliav, R. Benoliel, U. Herzberg, et al., The role of IL-6 and IL-1 beta in painful perineural inflammatory neuritis, Brain, Behav., Immun. 23 (2009) 474-484. https://doi.org/10.1016/j.bbi.2009.01.012.

[33] Y.N. Chen, M.R. Hu, L. Wang, et al., Macrophage M1/M2 polarization, Eur. J. Pharmacol. 877 (2020) 173090. https://doi.org/10.1016/j.ejphar.2020.173090.

[34] Y.H. Wang, W. Smith, D.J. Hao, et al., M1 and M2 macrophage polarization and potentially therapeutic naturally occurring compounds, Int. Immunopharmacol. 70 (2019) 459-466. https://doi.org/10.1016/j.intimp.2019.02.050.

[35] X.Y. Qi, L.L. Tong, H. Lian, et al., Selenium nanoparticles modified with Ophiocordyceps gracilis polysaccharides: Enhancing stability, bioavailability, and anti-inflammatory efficacy, Food Res. Int. 201 (2025) 115652. https://doi.org/10.1016/j.foodres.2024.115652.

[36] Y. Peng, M.X. Zhou, H. Yang, et al., Regulatory mechanism of M1/M2 macrophage polarization in the development of autoimmune diseases, Mediators Inflammation. 2023 (2023) 8821610. https://doi.org/10.1155/2023/8821610.

[37] S. Tardito, G. Martinelli, S. Soldano, et al., Macrophage M1/M2 polarization and rheumatoid arthritis: A systematic review, Autoimmun. Rev. 18 (2019) 102397. https://doi.org/10.1016/j.autrev.2019.102397.